JACS
JOURNAL OF THE AMERICAN CHEMICAL SOCIETY
Article
pubs.acs.org/JACS

Harvesting Singlet Fission for Solar Energy Conversion: One- versus Two-Electron Transfer from the Quantum Mechanical Superposition

Wai-Lun Chan,* John R. Tritsch, and X.-Y. Zhu*

Department of Chemistry & Biochemistry, University of Texas, Austin, Texas 78712, United States

Supporting Information

ABSTRACT: Singlet fission, the creation of two triplet excitons from one singlet exciton, is being explored to increase the efficiency of solar cells and photo detectors based on organic semiconductors, such as pentacene and tetracene. A key question is how to extract multiple electron−hole pairs from multiple excitons. Recent experiments in our laboratory on the pentacene/C_{60} system (Chan, W.-L.; et al. *Science* **2011**, *334*, 1543−1547) provided preliminary evidence for the extraction of two electrons from the multiexciton (ME) state resulting from singlet fission. The efficiency of multielectron transfer is expected to depend critically on other dynamic processes available to the singlet (S_1) and the ME, but little is known about these competing channels. Here we apply time-resolved photoemission spectroscopy to the tetracene/C_{60} interface to probe one- and two-electron transfer from S_1 and ME states, respectively. Unlike ultrafast (∼100 fs) singlet fission in pentacene where two-electron transfer from the multiexciton state resulting from singlet fission dominates, the relatively slow (∼7 ps) singlet fission in tetracene allows both one- and two-electron transfer from the S_1 and the ME states that are in a quantum mechanical superposition. We show evidence for the formation of two distinct charge transfer states due to electron transfer from photoexcited tetracene to the lowest unoccupied molecular orbital (LUMO) and the LUMO+1 levels in C_{60}, respectively. Kinetic analysis shows that ∼60% of the $S_1 \Leftrightarrow$ ME quantum superposition transfers one electron through the S_1 state to C_{60} while ∼40% undergoes two-electron transfer through the ME state. We discuss design principles at donor/acceptor interfaces for optimal multiple carrier extraction from singlet fission for solar energy conversion.

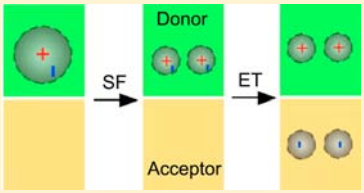

1. INTRODUCTION

The theoretical efficiency of a single-junction photovoltaic cell is limited to ∼31%, due in part to energy loss in the thermalization of hot excitons or carriers that are excited above the semiconductor bandgap.[1] One attractive proposal[2] to exceed this so-called Shockley−Queisser limit is to convert the excess energy of hot carriers into additional electron−hole pairs in a process called multiexciton generation (MEG).[3−5] While MEG is mainly found in nanomaterials, singlet fission (SF), a form of MEG, occurs in organic semiconductors.[6] Although MEG[7−9] or SF[10−12] can increase the quantum efficiency of solar cells and photodetectors, singlet fission is particularly attractive because of the highly reproducible nature of molecular materials and the prospects of designing and synthesizing molecules with optimal SF yields. In this study, we focus on the competition between singlet fission dynamics and electron transfer dynamics, and how they affect the efficiency of organic photovoltaics (OPVs).

In order to implement MEG or SF for enhanced quantum efficiency in photovoltaics, we must ensure that multiple electron/hole pair extraction from the MEG[7−9,13] or SF[10−12] chromophore is more competitive than single electron/hole pair extraction. This is not a trivial task because most efficient OPV cells are based on bulk heterojunctions consisting of nanoscopic phase-separated domains with high interfacial area.[14−16] A critical concern is that the majority of photogenerated excitons are close to the donor/acceptor interface and singlet exciton dissociation and electron transfer (ET) to the acceptor may out-compete singlet fission. The pentacene/C_{60} system in our recent study may be a pleasant exception, as the exothermic SF process in pentacene occurs on an ultrafast time scale (∼100 fs), faster than electron transfer to the C_{60} acceptor.[17] As a result, multiple electron transfer from the multiexciton state or triplet pair dominates interfacial ET. However, SF in other organic semiconductors may occur on much longer time scales. For example, in the most extensively studied system of crystalline tetracene, SF has been shown to occur on a few to a few hundred picoseconds.[6] Compared to pentacene, the much slower singlet fission in tetracene[18] provides an ample time window for us to probe dynamic channels that are competitive with the targeted multiple ET process. We choose the tetracene/C_{60} bilayer as the model system to compare with preliminary results on pentacene.[17] Tetracene/C_{60} multilayers have also been demonstrated in photodetectors with quantum efficiency exceeding 100%.[10]

In this work, we use time-resolved two-photon photoemission (TR-2PPE) spectroscopy to probe photoinduced ET at the tetracene/C_{60} interface. Unlike transient absorption and fluorescence spectroscopies that identify states based on resonances in photon energy, TR-2PPE spectroscopy identifies different excitonic states (singlet, multiexciton, triplets, and charge transfer) at the tetracene/C_{60} interface based on electron energies. TR-2PPE has the particular advantage of

Received: July 3, 2012
Published: October 15, 2012

   dx.doi.org/10.1021/ja306271y | J. Am. Chem. Soc. 2012, 134, 18295−18302

resolving the multiexciton state not observed in transient absorption or time-resolved fluorescence spectroscopy.

Before discussing multielectron extraction from pentacene or tetracene, it is important that we review the newly discovered singlet fission mechanisms in these two materials. As detailed elsewhere,[17,18] recent studies in our lab using TR-2PPE provided the first spectroscopic observation of the elusive ME intermediate state and revealed a coherent quantum coupling mechanism for singlet fission in pentacene and tetracene. Figure 1 shows pseudocolor plots of TR-2PPE spectra

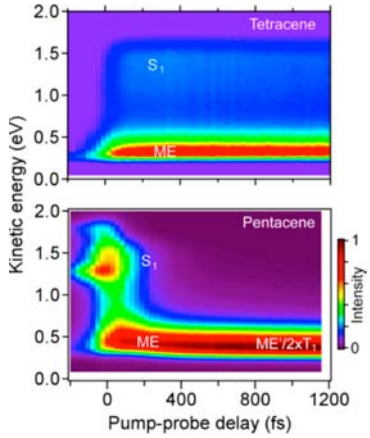

Figure 1. Pseudo color plots of TR-2PPE spectra of pentacene (lower) and tetracene (upper) thin films (≥15 nm).[17,18] Pentacene and tetracene are excited at $h\nu_1$ = 2.15 and 2.32 eV, respectively. In both experiments, the excitonic states are probed with an ionization photon energy of $h\nu_2$ = 4.65 eV. The energetic positions of the singlet (S_1), multiexciton (ME), and two triplets ($2\times T_1$) are indicated. Note that, in pentacene, the features near S_1 at negative pump−probe delays are charge transfer excitons on the surface of pentacene.[18]

(photoelectron energy versus pump−probe delay) for pentacene and tetracene films. In a TR-2PPE experiment, the pump laser pulse excites the material to create excitonic state(s); after a controlled time-delay, the probe laser pulse ionizes the excitonic states and the resulting photoelectrons are detected. Each two-dimensional plot reveals a high-energy feature assigned to the singlet state (S_1) and a lower energy one to the triplets (T_1). The most important finding is that a state at nearly the same energy as the triplets rises concurrently with S_1 upon photoexcitation. Since direct optical excitation of T_1 is forbidden, we assign the T_1-like state at early times to the multiexciton (ME) state, i.e., a correlated triplet pair. Note that the energy of the ME state is similar to that of S_1, but the photoionization step in the 2PPE process can only ionize one of the two excited electrons in the triplet pair and leave behind a triplet, leading to photoelectron energy from the ME state close to that from the T_1 state in a TR-2PPE spectrum.[17,18] The SF process can be summarized by the following equation:

$$[S_1 \Leftrightarrow ME] \xrightarrow{k_{SF}} ME' \rightarrow 2\times T_1 \quad (1)$$

The ME state is populated nearly instantaneously due to electronic coupling to the S_1 state, resulting in a quantum superposition state $S_1 \Leftrightarrow$ ME. Electronic decoupling occurs on a longer time scale and the superposition eventually turns into two triplets ($2\times T_1$) via an intermediate ME′, which is defined as two triplets mutually coupled electronically but decoupled from S_1. We define the fission rate (with rate constant k_{SF}) as the rate for the multiexciton state to lose its electronic coupling to the S_1 state.

The most notable difference between pentacene and tetracene is that the $S_1 \Leftrightarrow$ ME superposition state in pentacene has an extremely short lifetime (100 ± 20 fs),[17] while that in tetracene has a much longer one (7.2 ± 0.5 ps).[18] The ultrafast singlet fission process in pentacene can be attributed to strong electronic−nuclear interaction, leading to the energetic relaxation by 0.11 eV as the ME state is evolved into ME′/$2T_1$ (see lower panel in Figure 1). In tetracene, SF is endothermic and the ME is coupled to S_1 on a much longer time scale. Although the evolution of the S_1 population in tetracene measured in TR-2PPE is comparable to previous time-resolved absorption and fluorescent experiments,[19] our new definition (i.e., decoupling of the multiexciton state from the singlet) lowers the estimated time-scale for singlet fission from ∼100 ps to 7 ps. Note that the electronic coherence (between S_1 and ME) is very different than spin coherence (between two T_1 in the triplet pair state); the latter dephases on the much longer time scale of ns, as shown recently by Burdett and Bardeen.[20]

The drastically different lifetimes for $S_1 \Leftrightarrow$ ME in pentacene and tetracene have direct consequences on ET dynamics at their interfaces with the electron acceptor (C_{60}) although both crystalline pentacene and tetracene give similarly high SF yields.[2122] In pentacene, the extremely short lifetime of the [$S_1 \Leftrightarrow$ ME] superposition state is not affected even for 1 ML pentacene in direct contact with the electron acceptor C_{60}, indicating one-electron transfer from the pentacene S_1 state to C_{60} is not competitive on the 100 fs time scale.[17] Singlet fission in pentacene occurs faster than ET to C_{60} and two-electron transfer from the triplet pair (ME′ and $2\times T_1$) to C_{60} dominates (with time constants of 0.4 and 5 ps, respectively).[17] We find in the present study that this is not the case for tetracene: the relatively slow singlet fission process makes ET from both the singlet and the ME state competitive. Indeed, we find direct evidence for the formation of two distinct charge transfer states due to ET from the ME and the S_1 states in tetracene to the lowest unoccupied molecular orbital (LUMO) and the LUMO +1 levels, respectively, in C_{60}. The presence of one-electron transfer from S_1 before singlet fission lowers the quantum efficiency for charge carrier collection. This undesirable channel must be minimized if we are to obtain the highest quantum efficiency for charge carrier harvesting from singlet fission.

2. EXPERIMENTAL SECTION

All organic semiconductor thin film samples were grown by thermal evaporation in an ultrahigh vacuum (UHV) chamber with a base pressure of 3×10^{-9} Torr. We started with a Au(111) single crystal surface cleaned by standard sputtering (1 keV Ar, ∼5 μA cm^{-2}, 20 min) and annealing (770 K, 60 min) cycles. We followed a published procedure[23] to grow an epitaxial thin film of C_{60} (Sigma-Aldrich, 99.9% purity) with a nominal thickness of 5 monolayers (MLs) onto the Au(111) surface at elevated sample temperatures. The $(2\sqrt{3} \times 2\sqrt{3})$ R30° C_{60} superlattice was confirmed by low energy electron diffraction. Tetracene (Luminescence Technology, >99.5% purity) was vapor deposited on the crystalline C_{60} surface to give tetracene thicknesses ranging from 1 to 18 ML. Polyacenes grown on C_{60} are known to adopt bulk-like crystalline structure with the long axis of the molecules close to the surface normal.[24] In some experiment, we further deposited 1−2 ML C_{60} on top of the tetracene surface to form multilayer structures. After the deposition, the sample was transferred *in situ* to another UHV chamber (with a base pressure of 1×10^{-10} Torr), where the two-photon photoemission (2PPE) experiments were carried out.

dx.doi.org/10.1021/ja306271y | J. Am. Chem. Soc. 2012, 134, 18295−18302

In TR-2PPE experiment, the sample at ~180 K (cooled by liquid nitrogen) was excited by a visible pump laser pulse ($h\nu_1$ = 2.32 eV) from the output of an optical parametric oscillator (Coherent Mira-OPO). The temperature of the sample is measured by a thermocouple attached to the circumference of the Au substrate. The steady-state temperature of the substrate increases by ~20 K after laser irradiation. However, by solving the heat conduction equation, we estimate that the heat nonuniformity within the Au substrate and the organic layer is less than 1 K. The photon energy was chosen to match the first absorption peak in tetracene thin films.[25] The pulse energy and duration were 2 nJ and 100 fs, respectively. The excited electron was ionized by a time-delayed UV probe laser pulse ($h\nu_2$ = 4.65 eV, pulse energy = 0.25 nJ, pulse duration = 140 fs) which was frequency tripled from the output of the Ti:sapphire oscillator (Coherent Mira HP). The laser beam diameter had a full width at half-maximum of 0.35 mm at the sample surface. The repetition rate of the laser was 76 MHz. For experiments on the C_{60}/tetracene/C_{60}/Au(111) multilayer sample, the repetition rate of the laser was reduced to 3.8 MHz by a pair of pulse pickers (Conoptics 350-160-02) to avoid the buildup of a steady-state photoemission signal from residual electrons in the C_{60} layer (from charge separation) that did not recombine between two consecutive pulses. The photoelectrons were detected by a hemispherical electron energy analyzer (VG-Scienta R3000) with a 3 meV energy resolution. A sample bias of −2.5 V relative to the ground potential of the analyzer was applied to the electrically isolated sample during measurements. This bias is used to accelerate the photoelectrons from the sample to the entrance of the analyzer. We carried out ultraviolet photoelectron spectroscopy (UPS) measurement using the same electron energy analyzer as that in 2PPE. The UV light came from a He discharge source (VG) with a photon energy of $h\nu$ = 21.2 eV (He I line).

Note that the 2PPE technique probed mainly the topmost surface of the sample due to the finite electron escape depth.[17] For example, for pentacene films with thicknesses >2 ML deposited on C_{60}, we observed exclusively singlet fission dynamics, independent of film thickness. In the present study, we probed the charge transfer dynamics by reducing the tetracene thickess to ≤1 ML, i.e., in direct contact with the underlying C_{60} surface. Alternatively, we also monitored charge transfer dynamics using ~1 ML C_{60} deposited on top of a thick tetracene thin film; in this case, the 2PPE technique followed electron populations in the LUMO and LUMO+1 levels in charge transfer (CT) excitons formed from electron transfer from photoexcited tetracene to C_{60}.

In a typical 2PPE measurement, photoemission can also be induced by the UV pulse alone (without the pump pulse). This background signal can come from a number of sources, e.g., photoemission from residual excitons (triplets) that have not recombined within two sequential laser pulses, inelastic-scattered secondary electrons, or coherent two-photon photoemission from occupied states. In order to separate the pump-induced 2PPE signal (i.e., photoemission from excitons created by the pump pulse) from the background photoemission signal, we subtracted the photoemission spectrum at each delay time by the constant background obtained at long negative delay times. An example of the spectrum before and after subtraction is shown in the Supporting Information (Figure S1). As discussed in our previous work,[18] even if we assume that all background signals originated from unrecombined triplet excitons between laser pulses, the estimated density of the unrecombined exciton is on the order of ~(3−6) × 10^{16} excitations cm^{-3} (10−20% of the total excitation by the pump pulse). This low concentration of residue triplet excitons should not appreciably affect the ultrafast charge transfer and fission dynamics.

3. RESULTS AND DISCUSSION

To determine interfacial ET rates, we compare TR-2PPE spectra from a thick tetracene film (18 ML) with those of 1 ML tetracene on C_{60}. In the thick sample, TR-2PPE measures the SF dynamics on short time scales (7 ps) and slow recombination dynamics at longer times (~100 ps),[18] Figure 2a. For 1 ML tetracene in direct contact with C_{60}, we see rapid

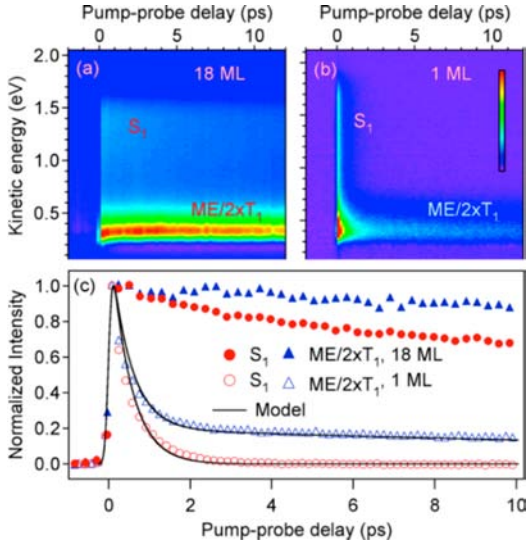

Figure 2. Pseudo color plots of 2PPE spectra of (a) 18 ML tetracene and (b) 1 ML tetracene deposited on the C_{60} surface. (c) Normalized intensities of the S_1 (circles) and ME/2×T_1 (triangles) peaks as a function of pump−probe delay time for 18 ML (solid) and 1 ML (open) tetracene on C_{60}. The data points are obtained from spectra in panels a and b. The solid lines are fits to the kinetic model described in the text.

decays in both S_1 and ME/2×T_1 signals, Figure 2b. We attribute the fast decays in exciton populations to ET from photoexcited tetracene to the C_{60} layer. Figure 2c shows normalized 2PPE intensities of S_1 and ME/2×T_1 peaks for both 1 and 18 ML tetracene. Note that we cannot directly separate the intensity contributions from the ME, ME′, and 2×T_1 states, since they appear in the same electron energy window in 2PPE spectra. This is in contrast to pentacene where there is energy relaxation as ME evolves into 2×T_1 via the intermediate ME′ state. However, we can distinguish the ME from the 2×T_1 state in tetracene based on fission dynamics,[18] or through the difference in their electron transfer rates, as detailed later. To simplify the kinetic analysis, we will not distinguish the correlated triplet pair (ME′) from the uncorrelated one (2×T_1) in eq 1 in terms of interfacial charge transfer dynamics. This simplification is justified as our previous experiment at the pentacene/C_{60} interface showed a nearly constant electron transfer rate from the triplet pairs to C_{60} at $t \geq 1$ ps. For tetracene, the coupled triplet pair (ME′) is formed on the longer time scale of 7 ps and likely resembles 2×T_1.

We now analyze the kinetics of interfacial ET. The S_1 and ME/2×T_1 populations decay with nearly the same rate for $t < 1$ ps. Experiments on thicker tetracene films show that the excitons are in the superposition [$S_1 \Leftrightarrow$ ME] state on this time scale and decoupling between the two occurs with a time constant of 7 ps.[18] The similar decays in S_1 and ME for $t < 1$ ps can be attributed to the constant ratio in their amplitudes due to a quantum superposition state formed between the two.[18] Under the quantum superposition model, each photoexcited exciton can either be an S_1 or ME state, with a probability amplitude predefined by the electronic coupling constant and density of states. A process such as interfacial electron transfer collapses the superposition wave function of a particular exciton into a charge transfer state, resulting in a loss in population of the [$S_1 \Leftrightarrow$ ME] coherent superposition state regardless of whether the incoherent charge transfer process occurs from S_1

dx.doi.org/10.1021/ja306271y | J. Am. Chem. Soc. 2012, 134, 18295−18302

or ME in the quantum superposition. For $t > 1$ ps, some of the ME excitons decouple electronically from S_1 to form two triplets (i.e., singlet fission) and the ME/2×T_1 population shows a much slower decay, similar to our earlier observation at the pentacene/C_{60} interface. Regardless of the similarity in the decay kinetics of ME/T_1 populations, there is a major difference between pentacene/C_{60} and tetracene/C_{60} interfaces. In tetracene, the superposition state is relative long-lived (7 ps) and the ME state is electronically coupled to S_1 during electron transfer, allowing both the S_1 state and the ME state to transfer electron(s) to C_{60}. In pentacene, the superposition state is short-lived (~100 fs) and electron transfer occurs on the longer time scale of ~400 fs, mostly from the ME′ state that is electronically decoupled from the S_1.[17] To construct the kinetic model, we define a joint population for the superposition $S_1 \Leftrightarrow$ ME state:

$$[S_1 \Leftrightarrow ME] = [S_1] + [ME] \quad (2)$$

The fast electronic coupling between S_1 and ME is accounted for by fixing the fraction of each state in the superposition: $[S_1]/([ME] + [S_1]) = f_{S_1}$, where f_{S_1} is the fraction of population in the S_1 state and is a constant. As discussed above, there is no need to assign individual decay rates to the S_1 and ME states. We define a joint decay rate for the superposition state, which includes contributions from SF and interfacial ET with rate constants of k_{SF} and k_{ET1}, respectively. For the 2×T_1 state, the electron transfer rate constant is k_{ET2}. We can write down the time-dependent equations for the exciton populations as

$$d[S_1 \Leftrightarrow ME]/dt = \alpha I_{h\nu_1}(t)/h\nu_1 - k_{SF}[S_1 \Leftrightarrow ME] - k_{ET1}[S_1 \Leftrightarrow ME] \quad (3)$$

$$d[T_1]/dt = 2k_{SF}[S_1 \Leftrightarrow ME] - k_{ET2}[T_1] \quad (4)$$

Here, $I_{h\nu}$ is the pump laser fluence, α is the linear optical absorption coefficient, and $[T_1]$ is the T_1 population. The intensities of the S_1 and ME/T_1 peaks are taken to be $I_{S_1} \propto [S_1]$ and $I_{ME/2\times T_1} \propto 2[ME] + [T_1]$, respectively. Equations 3 and 4 can be solved analytically by using a delta function for $I_{h\nu_1}(t)$.[17] Fitting the experimental data to this kinetic model and convoluting the solution with the finite pulse duration gives the solid lines shown in Figure 2c. To give a singlet fission time constant of $\tau_{SF} = 1/k_{SF} \sim 7$ ps as determined previously,[18] we find the f_{S_1} value needs to be ~0.5. The f_{S_1} value obtained from kinetic fitting is consistent with results from quantum mechanical modeling,[17,18] where we find that the time-averaged populations of the S_1 and ME states are equal. The time constants for ET from the superposition state and from the T_1 state are $\tau_{ET1} = 1/k_{ET1} = 0.5$ ps and $\tau_{ET2} = 1/k_{ET2} = 26$ ps, respectively. The former is very similar to the time constant for ET from the ME/ME′ states at the pentacene/C_{60} interface.[17]

As we discussed earlier, singlet fission in tetracene is temperature independent.[18] We find that electron transfer at the tetracene/C_{60} interface is also temperature independent, as shown in Figure 3 for the time profiles of both the S_1 (left) and ME/2×T_1 (right) populations. Thus, interfacial electron transfer from photoexcited tetracene to C_{60} is not thermally activated. The lack of thermal activation may be attributed to strong electronic coupling as well as the presence of a high density of states at the condensed matter interface.[26]

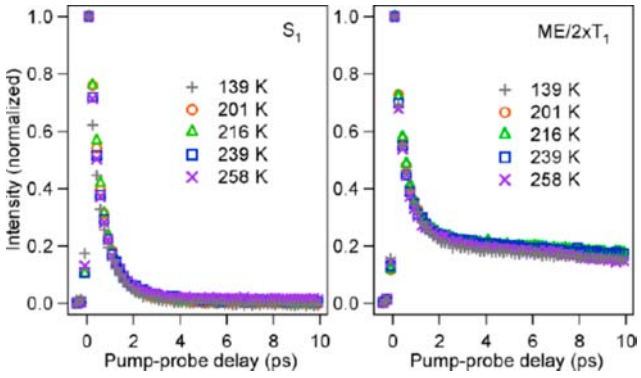

Figure 3. Normalized intensities (dots) of the S_1 (left) and ME/2T_1 (right) peaks in TR-2PPE spectra from 1 ML tetracene deposited on the C_{60} surface as a function of pump−probe delay time for five different sample temperatures (139−258 K).

In the above kinetic analysis, we obtain a total rate of ET from the $S_1 \Leftrightarrow$ ME superposition state to the C_{60} electron acceptor layer. A critical question remains: *Does ET occur from the S_1 state or the ME state?* The former corresponds to one-electron transfer, while the latter gives two.[17] To distinguish these two ET channels, we directly probe the charge transfer (CT) excitons resulting from interfacial ET. Each interfacial CT exciton essentially consists of an electron (e) on the acceptor molecule (C_{60}) and a hole (h) on the donor molecule (tetracene), with the e−h pair bound by the Coulomb potential across the donor/acceptor interface. Because of the different energies between singlet and triplet states in tetracene, we expect the CT excitons from the S_1 and ME states (a correlated triplet pair) to involve different C_{60} electron acceptor levels that may be resolved in TR-2PPE spectra. In this set of experiments, we deposit a thin C_{60} film in the monolayer coverage region on top of a thick tetracene thin film. TR-2PPE spectroscopy is ideally suited for the detection of the interfacial CT exciton states because the photoemission technique preferentially probes the topmost surface of the sample due to the finite escape depth of low energy photoelectrons. As a result, TR-2PPE should be most sensitive to a CT exciton state with the transient electron on the C_{60} side (surface).

Figure 4a and b show the TR-2PPE spectra from a single layer of C_{60} thin film (5 ML) on Au and a monolayer C_{60} thin film deposited on a thick (18 ML) tetracene thin film. For C_{60} only, there is very weak pump-induced intensity near time zero, which may be attributed to coherent two-photon (pump + probe) ionization of the highest occupied molecular orbital (HOMO).[23] In contrast, when the C_{60} layer is deposited on top of tetracene, we observe clear pump-induced photoemission intensities across a broad energy range. At $h\nu_1 = 2.32$ eV, the pump-photon is strongly absorbed by the tetracene below the C_{60} surface layer, but ionization by the probe photon ($h\nu_2 = 4.65$ eV) shows strong photoemission intensity from the C_{60} surface. Since the results in Figure 2b suggest efficient electron transfer from photoexcited tetracene to C_{60}, we assign the 2PPE spectral features in Figure 4b as resulting from the photo-ionization (by $h\nu_2$) of interfacial CT excitons. The presence of two distinct spectral features suggests the presence of two different CT excitons. This assignment is most obvious when we take vertical cuts of the data in Figure 4b, i.e., photoelectron spectra (intensity vs electron energy) at different pump−probe delay times, Figure 4c. There are clearly two photoelectron peaks corresponding to the two interfacial CT excitons. Since

dx.doi.org/10.1021/ja306271y | J. Am. Chem. Soc. 2012, 134, 18295−18302

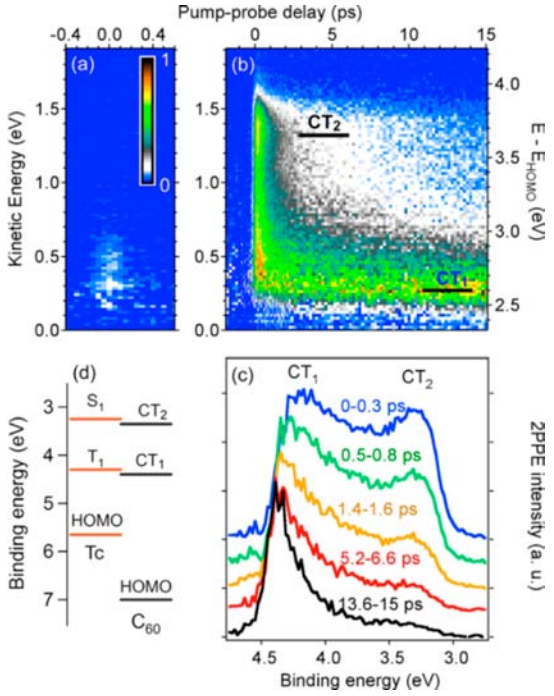

Figure 4. Pseudo color representation of TR-2PPE spectra from (a) C_{60} (5 ML) on Au(111) and (b) ~monolayer C_{60} on tetracene. The pump and probe photon energies are $h\nu_1$ = 2.32 eV and $h\nu_2$ = 4.65 eV, respectively. Panel c shows a series of TR-2PPE spectra, i.e., vertical cuts from panel b, integrated over the indicated windows of pump−probe delay times. Panel d shows energy level alignment (in units of electron binding energy for photoionization) of the singlet (S_1), the triplet (T_1), the HOMO of tetracene (Tc), the HOMO of C_{60}, and two CT excitons (CT_1 and CT_2) involving and LUMO and LUMO+1 of C_{60}. The HOMO levels are from UPS spectra in Figure 5.

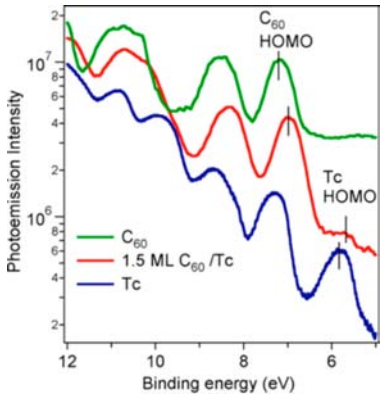

Figure 5. Ultraviolet photoelectron spectra (UPS) for (i) a 5 ML C_{60} thin film (green), (ii) an 18 ML tetracene (Tc) thin film (blue), and (iii) ~1.5 ML C_{60} deposited on 18 ML tetracene (red). Note that the binding energy scale is referenced to the vacuum level here for convenient comparison to 2PPE spectra (see Figure 4).

the energetic separation between these two states is close to the energy gap between the two negative ion states of C_{60} involving LUMO and LUMO+1,[27] we assign these states to interfacial CT excitons, CT_1 and CT_2, with the electron on C_{60} in the LUMO and LUMO+1 orbitals, respectively. This assignment is further supported by the binding energies of the CT excitons. Figure 4d shows the photoelectron binding energies of these excited states (with respect to the vacuum level) obtained from TR-2PPE spectra, along with those of the highest occupied molecular orbital (HOMO) measured by ultraviolet photoemission spectroscopy (Figure 5). The CT_1 and CT_2 states are located above the highest occupied molecular orbital (HOMO) of C_{60} by 2.6 ± 0.2 and 3.7 eV ± 0.2 eV, respectively. These energy gaps are lower than the transport gaps (3.4 and 4.6 eV, respectively)[28] by the exciton binding energies: BE_{CT1} = 0.8 eV and BE_{CT2} = 0.9 eV. For comparison, the optical gaps of C_{60} are 1.8 and 2.7 eV for the HOMO → LUMO and HOMO → LUMO+1 transitions,[29,30] corresponding to Frenkel exciton binding energies of BE_{FE1} = 1.6 eV and BE_{FE2} = 1.9 eV, respectively. Thus, the binding energies of CT excitons are about half of those of Frenkel excitons. This is expected because the electron−hole separation in an interfacial CT exciton (with electron on a C_{60} and hole on a tetracene molecule) should be larger than that of an on-molecule Frenkel exciton (both electron and hole on the same C_{60} molecule).

Since S_1 and ME/2×T_1 are nearly resonant in energy with CT_2 and CT_1, respectively, we attribute the formation of CT_2 as resulting from electron transfer from the singlet exciton (S_1) in tetracene to the C_{60} LUMO+1, and that of CT_1 due to electron transfer from the triplet pair (ME/2×T_1) to the C_{60} LUMO. Note that, although the ME state is energetically close to the S_1 state, it consists of two excited electron−hole pairs and each of the excitons is energetically in resonance with the T_1 state (Figure 4d). Therefore, similar to T_1, the ME transfers its excited electrons to the lower LUMO level of C_{60}. In addition to ultrafast electron transfer and CT exciton formation, the results in Figure 4c also reveal relaxation dynamics in the CT exciton manifold on a slower time scale: the intensity of the higher energy CT_2 peak decreases on a picosecond time scale, while that of the lower energy CT_1 peak increases correspondingly. To quantitatively analyze the CT exciton dynamics, we assume all the CT excitons observed are due to direct electron transfer from tetracene to C_{60} at or near the interface. Excitons generated in tetracene further away from the interface can, in principle, diffuse toward to the interface and participate in electron transfer. However, this involves exciton diffusion in the direction along the *c*-axis of the crystalline tetracene and occurs on a longer time scale of ~100 ps for diffusing over a distance of only a few monolayers.[6] Thus, on the time scale of our measurement (~10 ps), the CT excitons originate mostly from direct electron transfer at the interface. Note that, in our experiments, we use samples with ultrathin C_{60} layers (~1 ML) because of limitations of the photoemission technique. The thin C_{60} film confines the CT exciton to the interface. A thicker C_{60} layer may allow electronic delocalization and the formation of hot CT excitons with reduced binding energy, thus promoting charge separation.[31] This issue is beyond the scope of the current study and deserves further investigation.

We can model the populations of the two CT excitons, $[CT_1]$ and $[CT_2]$, by

$$d[CT_2]/dt = k_{CT2}[S_1 \Leftrightarrow ME] - k_r[CT_2] \quad (5)$$

$$d[CT_1]/dt = 2k_{CT1}[S_1 \Leftrightarrow ME] + k_{ET2}[T_1] + k_r[CT_2] \quad (6)$$

where k_{CT2} and k_{CT1} are rate constants for electron transfer from the S_1 and ME to form CT_2 and CT_1, respectively; k_r is the rate constant for relaxation from CT_2 to CT_1. The individual electron transfer rate constants from S_1 and ME

dx.doi.org/10.1021/ja306271y | J. Am. Chem. Soc. 2012, 134, 18295−18302

states are related to the overall population decay rate constant of the quantum superposition $S_1 \Leftrightarrow$ ME:

$$k_{CT2} = fk_{ET1}, \quad k_{CT1} = (1-f)k_{ET1} \tag{7}$$

where the parameter f is the fraction of the decay rate from the $S_1 \Leftrightarrow$ ME superposition to form the hot CT_2 exciton and $(1-f)$ is that for the CT_1 exciton. To compare the experimental data to the kinetic model in eqs 5 and 6, we also need to take into account the fact that photoemission intensities from photoexcited tetracene underneath the surface are not completely attenuated by the C_{60} thin film. The TR-2PPE intensities from the interfacial charge transfer excitons, CT_2 and CT_1, cannot be resolved energetically from the S_1 and ME/$2xT_1$ states, respectively, in tetracene. Thus, the higher energy peak in TR-2PPE spectra (labeled CT_2 in Figure 4) and the lower energy peak (labeled CT_1 in Figure 4) can be represented as $I_h = A_1[CT_2] + A_2[S_1]$ and $I_l = A_3[CT_1] + A_4(2[ME] + [T_1])$, respectively, where A_1, A_2, A_3, and A_4 are scaling constants.

Figure 6 shows the time evolution of the photoemission intensities. The experimental data are shown as open squares

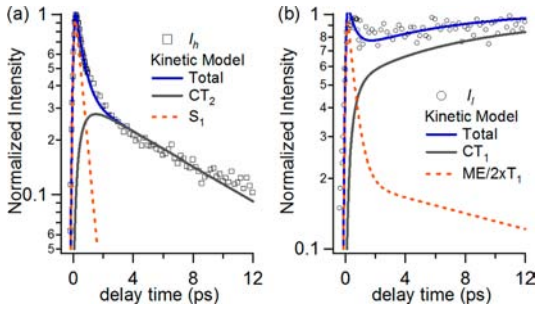

Figure 6. The intensities of the (a) S_1/CT_2 peak and (b) $ME/T_1/CT_1$ peaks as a function of pump−probe delay times for the spectrum shown in Figure 4b. The blue solid lines are results from the model. Contributions from the C_{60} and the tetracene layers are indicated by solid gray and red-dashed lines, respectively.

(I_h) and circles (I_l) compared to the simulated dynamics from the kinetic model as solid blue lines. In the model, we fix all kinetic parameters (k_{SF}, k_{ET1}, and k_{ET2}) obtained earlier in fitting to results in Figure 2 and only vary the parameters k_r (relaxation of CT_2 from CT_1) and the relative rate fraction f (forming the hot CT_2 exciton), as well as the A_{1-4} parameters to account for the mixing of the tetracene signal and CT exciton signal. At short delay times ($t < 1$ ps), a major part of the intensities originates from the tetracene layer (red dashed lines), while, at longer delay times, the signals from CT excitons (gray curves) due to electron transfer from tetracene to the LUMO+1 and LUMO levels of C_{60} dominate. The rate k_r can be determined from the decay rate of CT_2 and the rise time of CT_1 for $t > 2$ ps (Figure 6). The rise and decay in the population of the CT_2 state are due to electron transfer from tetracene S_1 to the LUMO+1 of C_{60} and the subsequent relaxation of CT_2 to the CT_1 state. For the CT_1 state, we see two rises with different time constants. The initial rapid rise is due to the direct electron transfer from the ME state of tetracene to C_{60}, while the slower rise results from the relaxation of CT_2 to CT_1. From the amplitude ratio of the slower rise and the initial rapid rise, we can determine the parameter f in eq 7. The lines shown in Figure 6 are calculated with $f = 0.6$, i.e., 60% of electron transfer is through the singlet exciton (S_1), producing one CT exciton per absorbed photon, and 40% is through the triplet pair (ME), which produces two CT excitons per absorbed photon. This corresponds to a carrier extraction yield of 140%. Equation 8 summarizes the fission, CT, and exciton relaxation processes at the tetracene/C_{60} interface:

$$\begin{array}{ccccc} [S_1 \Leftrightarrow ME] & \xrightarrow[ps^{-1}]{0.15} & 2\times T_1 \\ \downarrow 1.2 & \searrow 0.8 & \downarrow 0.04 \\ CT_2 & \xrightarrow{0.11} & CT_1 \end{array} \tag{8}$$

where all rate constants are in units of ps^{-1}. We note that, in this model, the absolute values for A_{1-4} are not important, since the intensities in Figure 6 are normalized. The ratios A_1/A_2 and A_3/A_4, however, represent the signal contribution from the C_{60} relative to the tetracene layer at different photoelectron energies. The model agrees well with the experiment for A_1/A_2 and A_3/A_4 to be 0.44 and 0.56, respectively. From repeated modeling by varying the kinetic parameters, we estimate an error range of ±15% for the parameters in eq 8.

To demonstrate the quality of the kinetic modeling, we use the kinetic parameters from eq 8 to reconstruct the complete 2PPE spectrum as a function of energy and time. We determine the spectral line-shapes of different states by fitting the spectra at different regions of the 2PPE spectrum (see the Supporting Information for details) where the intensity from a single state is dominant. These results are shown in the Supporting Information, Figures S2 anmd S3. The reconstructed spectrum captures the major features observed in the experimental spectrum (Figure S2, Supporting Information). The energetic position of the spectrum for each state (Figure S3c, Supporting Information) also agrees well with the energy-level assignment shown in Figure 4d. The model also shows good agreement with the experimental spectrum at different delay times (Figure S3, Supporting Information). Our analysis demonstrates that the kinetic scheme used in eq 8 can generate a 2PPE spectrum that agrees quantitatively with experimental data in a self-consistent way.

In eq 8, the dominant charge transfer processes are from the quantum mechanical superposition state, $S_1 \Leftrightarrow$ ME, which allows one-electron transfer from S_1 to the C_{60} LUMO+1 to form CT_2 and two-electron transfer from ME to the C_{60} LUMO to form two CT_1 states. Such a competing one- vs two-electron transfer scenario is in stark contrast to the pentacene/C_{60} interface, where the dominant charge transfer process is not from the $S_1 \Leftrightarrow$ ME quantum superposition but from the triplet pair state ME′. This is due to the ultrafast singlet fission process which decouples the triplet pair from S_1 before electron transfer occurs. However, the favorable scenario for multicarrier harvesting in pentacene is an exception, rather than the norm, as singlet fission processes in other known systems, including tetracene,[18,22] 1,3-diphenylisobenzofuran,[32] rubrene,[33] and 5,12-diphenyltetracene,[34] occur on slower time-scales of ∼1−100 ps where competitive one- vs two-electron transfer must be considered. The findings presented above suggest important design principles for the efficient harvesting of multiple carriers from singlet fission:

- *Singlet fission faster than electron transfer*. Ideally, we would prefer an ultrafast singlet fission process occurring faster than interfacial electron transfer to minimize the possible one-electron transfer from the singlet state. This is likely the case at the pentacene/C_{60} interface, where the singlet fission rate is ∼10 ps^{-1}, which is 4 times faster than the interfacial electron

dx.doi.org/10.1021/ja306271y | J. Am. Chem. Soc. 2012, 134, 18295−18302

transfer rate of ~2.5 ps^{-1} (measured for the ME′ state).[17] The ultrafast singlet fission in pentacene may result from a barrierless transition (see ref 17 and references cited therein).

• *Limiting interfacial charge transfer*. Since charge transfer is expected to occur only at the donor−acceptor interface, one may use a thicker donor layer or decrease the concentration of the acceptors to slow down charge transfer rates relative to the singlet fission rate. In this scenario, the product of singlet fission, i.e., triplets, must undergo the slow triplet diffusion process to reach the donor−acceptor interface for charge separation. However, there are also disadvantages with such a strategy, as the slow triplet diffusion process may make loss channels, such as triplet−triplet annihilation and recombination, competitive.

• *Energy selective electron transfer from the ME state*. In the case of slow singlet fission, efficient multicarrier extraction is still possible if two-electron transfer from the ME state is more competitive than one-electron transfer from the S_1 state in the $S_1 \Leftrightarrow$ ME superposition. This may be possible when there is an acceptor level for resonant electron transfer from the ME state (triplet pair) to the electron acceptor but not for that from the S_1 state. This is not the case for the tetracene/C_{60} interface presented here, as the LUMO+1 and LUMO levels in C_{60} are nearly resonant with the tetracene singlet and triplet states, respectively. Note that this strategy only works in the limit of strong electronic coupling when thermal activation is not important. For thermally activated electron transfer in the weak electronic coupling limit, the reduction in electronic coupling strength due to a loss of resonance could be compensated for by a larger energetic driving force, thus making selective electron transfer ineffective.

• *Enhancing the carrier multiplication yield by electron transfer*. The discovery of the $S_1 \Leftrightarrow$ ME superposition state in singlet fission opens the door to a new channel for efficient multicarrier extraction, even though the singlet fission yield may be intrinsically low. As suggested by Shabaev et al.,[35] the yield for multicarrier extraction from the quantum superposition state [$S_1 \Leftrightarrow$ ME] can be represented as

$$\frac{N_{ME}}{N_{S_1}} = P_{1\to 2}\frac{\gamma_2}{\gamma_1} \tag{9}$$

where N_{ME} and N_{S_1} are the numbers of electrons extracted through the ME and S_1 states, respectively, and $P_{1\to 2}$ is the transition probability from the S_1 to ME via coherent electronic coupling. The rates γ_2 and γ_1 are the incoherent decay rates from ME and S_1, respectively. Either γ_2 or γ_1 can be represented as a sum of radiative/nonradiative recombination rate and electron transfer rate (to an acceptor). If the rate of two-electron transfer from the ME state is optimized due to energy resonance with an electron acceptor, γ_2 is increased. Therefore, the effective multicarrier extraction yield can be larger than the intrinsic fission yield, provided that $\gamma_2 \gg \gamma_1$ and the superposition state has a long enough lifetime for electron transfer to occur.

4. CONCLUSION

We have determined the critical competition between one- and two-electron transfer at the model singlet fission donor/electron acceptor interface of tetracene/C_{60}. These results are contrasted with those at the pentacene/C_{60} interface where singlet fission out-competes interfacial electron transfer and two-electron transfer dominates. At the tetracene/C_{60} interface, the relatively slow singlet fission process in tetracene leads to dominant charge transfer events proceeding through the quantum superposition state $S_1 \Leftrightarrow$ ME. We show that ~60% of the $S_1 \Leftrightarrow$ ME superposition undergoes one-electron transfer from S_1 and ~40% via two-electron transfer from ME, leading to the formation of hot and cold charge transfer excitons (CT_2 and CT_1), respectively, at the tetracene/C_{60} interface. While ultrafast singlet fission occurring faster than electron transfer (to acceptors) may be preferred for the harvesting of multicarriers, efficient harvesting of two electrons from the singlet fission chromorphore may also be achieved when singlet fission occurs slower than electron transfer. In the latter case, one- and two-electron transfer occur competitively from the $S_1 \Leftrightarrow$ ME quantum superposition state. Two-electron transfer may be selectively optimized when acceptor electronic levels are resonant with each triplet in the ME state but not with the S_1 state. The preferential electron transfer from the ME state in the $S_1 \Leftrightarrow$ ME superposition can enhance the effective carrier-extraction yield beyond the intrinsic singlet fission yield.

■ ASSOCIATED CONTENT

Supporting Information

A 2PPE spectrum before background subtraction; a 2-D modeling for the C_{60} on the tetracene spectrum. This material is available free of charge via the Internet at http://pubs.acs.org.

■ AUTHOR INFORMATION

Corresponding Author

xyzhu@columbia.edu (X.-Y.Z); wlchan@ku.edu (W.-L.C.)

Notes

The authors declare no competing financial interest.

■ ACKNOWLEDGMENTS

This work was solely supported as part of the program "Center for Re-Defining Photovoltaic Efficiency Through Molecule Scale Control", an Energy Frontier Research Center funded by the U.S. Department of Energy, Office of Science, Office of Basic Energy Sciences under Award Number DE-SC0001085.

■ REFERENCES

(1) Shockley, W.; Queisser, H. J. *J. Appl. Phys.* **1961**, *32*, 510−519.
(2) Hanna, M. C.; Nozik, A. J. *J. Appl. Phys.* **2006**, *100*, 074510.
(3) McGuire, J. A.; Joo, J.; Pietryga, J. M.; Schaller, R. D.; Klimov, V. I. *Acc. Chem. Res.* **2008**, *41*, 1810−1819.
(4) Beard, M. C.; Midgett, A. G.; Hanna, M. C.; Luther, J. M.; Hughes, B. K.; Nozik, A. J. *Nano Lett.* **2010**, *10*, 3019−3027.
(5) Gabor, N. M.; Zhong, Z.; Bosnick, K.; Park, J.; McEuen, P. L. *Science* **2009**, *325*, 1367−1371.
(6) Smith, M. B.; Michl, J. *Chem. Rev.* **2010**, *110*, 6891−6936.
(7) Semonin, O. E.; Luther, J. M.; Choi, S.; Chen, H.-Y.; Gao, J.; Nozik, A. J.; Beard, M. C. *Science* **2011**, *334*, 1530−1533.
(8) Sambur, J. B.; Novet, T.; Parkinson, B. A. *Science* **2010**, *330*, 63−66.
(9) Sukhovatkin, V.; Hinds, S.; Brzozowski, L.; Sargent, E. H. *Science* **2009**, *324*, 1542−1545.
(10) Jadhav, P. J.; Mohanty, A.; Sussman, J.; Lee, J.; Baldo, M. A. *Nano Lett.* **2011**, *11*, 1495−1498.
(11) Ehrler, B.; Wilson, M. W. B.; Rao, A.; Friend, R. H.; Greenham, N. C. *Nano Lett.* **2012**, *12*, 1053−1057.
(12) Lee, J.; Jadhav, P.; Baldo, M. A. *Appl. Phys. Lett.* **2009**, *95*, 033301.
(13) Huang, J.; Huang, Z.; Yang, Y.; Zhu, H.; Lian, T. *J. Am. Chem. Soc.* **2010**, *132*, 4858−4864.

(14) Yu, G.; Gao, J.; Hummelen, J. C.; Wudi, F.; Heeger, A. J. *Science* **1995**, *270*, 1789−1791.
(15) Brabec, C. J.; Gowrisanker, S.; Halls, J. J. M.; Laird, D.; Jia, S.; Williams, S. P. *Adv. Mater.* **2010**, *22*, 3839−3856.
(16) Sun, Y.; Welch, G. C.; Leong, W. L.; Takacs, C. J.; Bazan, G. C.; Heeger, A. J. *Nat. Mater.* **2012**, *11*, 44−48.
(17) Chan, W.-L.; Ligges, M.; Jailaubekov, A.; Kaake, L.; Miaja-Avila, L.; Zhu, X.-Y. *Science* **2011**, *334*, 1541−1545.
(18) Chan, W.-L.; Ligges, M.; Zhu, X.-Y. *Nat. Chem.* **2012**, *4*, 840−845.
(19) Burdett, J. J.; Gosztola, D.; Bardeen, C. J. *J. Chem. Phys.* **2011**, *135*, 214508.
(20) Burdett, J. J.; Bardeen, C. J. *J. Am. Chem. Soc.* **2012**, *134*, 8597.
(21) Rao, A.; Wilson, M. W. B.; Hodgkiss, J. M.; Albert-Seifried, S.; Bassler, H.; Friend, R. H. *J. Am. Chem. Soc.* **2010**, *132*, 12698−12703.
(22) Burdett, J. J.; Müller, A. M.; Gosztola, D.; Bardeen, C. J. *J. Chem. Phys.* **2010**, *133*, 144506.
(23) Dutton, G.; Quinn, D. P.; Lindstrom, C. D.; Zhu, X.-Y. *Phys. Rev. B* **2005**, *72*, 045441.
(24) Dougherty, D. B.; Jin, W.; Cullen, W. G.; Reutt-Robey, J. E.; Robey, S. W. *Appl. Phys. Lett.* **2009**, *94*, 023103.
(25) Yamagata, H.; Norton, J.; Hontz, E.; Olivier, Y.; Beljonne, D.; Brédas, J. L.; Silbey, R. J.; Spano, F. C. *J. Chem. Phys.* **2011**, *134*, 204703.
(26) Sánchez-Portal, D.; Stähler, J.; Zhu, X.-Y. Basic theory of heterogeneous electron transfer. In *Dynamics at Solid State Surfaces and Interfaces, Part II: Fundamentals*; Bovensiepen, U., Petek, H., Wolf, M., Ed.; Wiley-VCH: Berlin, 2012. ISBN: 978-3-527-40924-2.
(27) Schwedhelm, R.; Kipp, L.; Dallmeyer, A.; Skibowski, M. *Phys. Rev. B* **1998**, *58*, 13176−13180.
(28) Rudolf, R.; Golden, M. S.; Brühwiler, P. A. *J. Electron Spectrosc. Relat. Phenom.* **1999**, *100*, 409−433.
(29) Reber, C.; Yee, L.; McKiernan, J.; Zink, J. I.; Williams, R. S.; Tong, W. M.; Ohlberg, D. A. A.; Whetten, R. L.; Diederich, F. *J. Phys. Chem.* **1991**, *95*, 2127−2129.
(30) Lof, R. W.; van Veenendaal, M. A.; Koopmans, B.; Jonkman, H. T.; Sawatzky, G. A. *Phys. Rev. Lett.* **1992**, *68*, 3924−3927.
(31) Bakulin, A. A.; et al. *Science* **2012**, *335*, 1340−1344.
(32) Johnson, J. C.; Nozik, A. J.; Michl, J. *J. Am. Chem. Soc.* **2010**, *132*, 16302−16303.
(33) Ma, L.; Zhang, K.; Kloc, C.; Sun, H.; Michel-Beyerle, M. E.; Gurzadyan, G. G. *Phys. Chem. Chem. Phys.* **2012**, in press.
(34) Roberts, S. R.; McAnally, R. E.; Mastron, J. N.; Webber, D. H.; Whited, M. T.; Brutchey, R. L.; Thompson, M. E.; Bradforth, S. E. *J. Am. Chem. Soc.* **2012**, *134*, 6388−6400.
(35) Shabaev, A.; Efros, Al. L.; Nozik, A. J. *Nano Lett.* **2006**, *6*, 2856−2863.